Lasers Med Sci (2015) 30:1923–1929
DOI 10.1007/s10103-015-1784-8

ORIGINAL ARTICLE

Topical antimicrobial photodynamic therapy improves angiogenesis in wounds of diabetic mice

Khageswar Sahu[1] · **Mrinalini Sharma**[1] · **Alok Dube**[1] · **Pradeep Kumar Gupta**[1]

Received: 20 February 2015 / Accepted: 22 June 2015 / Published online: 10 July 2015

Abstract We report the results of our investigations on the effect of antimicrobial photodynamic therapy (APDT) on angiogenesis in wounds of diabetic mice. For this, measurements were made on levels of nitric oxide (NO), vascular endothelial growth factor-A (VEGF-A), and markers of pro-inflammatory stress (phosphorylated nuclear factor kappa B and p^{38} mitogen-activated protein kinase) on day 3 post-wounding. For uninfected and infected wounds, the levels of NO, VEGF-A were lower and the levels of phospho-NF-kB-p65, phospho-p^{38}MAPK were higher in diabetic mice compared with that in nondiabetic mice. For infected wounds, multiple APDT (fluence ~60 J/cm^2) led to increase in NO, VEGF-A levels and a decrease in the phospho-NF-kB-p65, phospho-p^{38}MAPK. Further, compared with aminoguanidine, and silver nitrate, multiple APDT was observed to result in a much improved proangiogenic response.

Keywords Antimicrobial photodynamic therapy · Diabetes · Chronic wounds · Angiogenesis · Nitric oxide · Vascular endothelial growth factor

Introduction

Antimicrobial photodynamic therapy (APDT), which makes use of photoexcitation of a photosensitive drug to inactivate bacteria is receiving a lot of attention for the management of antibiotic-resistant bacteria infection in wounds [1–3]. PDT, in addition to the antibacterial effect, has also been shown to have influence on several other factors like bacterial toxins [4], proinflammatory cytokines [5], matrix metalloproteases, collagen synthesis, and remodeling [6] in wounds. Therefore, APDT appears promising for the treatment of diabetic wounds where healing is impaired and the treatment is further complicated by bacterial infection [7–9]. An important cause for impaired healing in diabetes is reduced angiogenesis [10, 11] which is primarily caused by reduced arteriogenic response of monocyte/macrophages in the wound [12]. Although, the enhancement in angiogenesis in tumor by PDT has been reported [13], so far, the effect of APDT on angiogenesis process of diabetic wound has not received attention.

In this study, we investigated the influence of poly-L-lysine-conjugated chlorin p6 (pl-cp6) mediated APDT on angiogenesis in wounds of diabetic mice. Chlorin p6, a cholorophyll derivative, is a promising photosensitizer as it has strong absorbance in the red (660 nm) region and good triplet yield [14]. Since cp6 is anionic, it was conjugated with cationic peptide poly-L-lysine to enhance the targeting to both gram-positive and gram-negative bacterial cells. Our previous studies on pl-cp6-mediated PDT have shown it to be a very efficient antimicrobial photodynamic agent [5, 6]. Effect of PDT on angiogenesis was evaluated by monitoring the levels of nitric oxide (NO) and vascular endothelial growth factor-A (VEGF-A). Also, effect of PDT on level of inflammatory stress markers, phosphorylated nuclear factor kaapa B (phospho-NF-kB-p65) and p^{38} mitogen-activated protein kinase (phospho-p^{38} MAPK) were monitored, since expression of these factors are influenced by diabetes [15, 16], bacteria infection [17], and ROS [18, 19]. Further, the efficacy of APDT has been compared with that of aminoguanidine (AG), an inhibitor of advanced glycated end products which

✉ Khageswar Sahu
khageswar@rrcat.gov.in; khageswar80@gmail.com

[1] Laser Biomedical Applications and Instrumentation Division, R&D Block-D, Raja Ramanna Centre for Advanced Technology, Indore 452 013, Madhya Pradesh, India

play an important role in the pathogenesis of diabetic complications [20, 21] and silver nitrate ($AgNO_3$), an antibacterial agent [22].

Material and methods

Bacterial strain and growth conditions

The methicilin resistant *Staphylococcus aureus* (MRSA) strain used in this study (ATCC 43300) was maintained routinely by sub culturing in tryptone soya broth (TSB, Himedia, Mumbai, India). For experiments, a colony of the bacteria was inoculated in TSB and was grown aerobically for 18 h at 37 °C using a shaker incubator. For studies on wounds, optical density of the overnight culture of bacteria was measured at 600 nm using a spectrophotometer (Cintra 20, GBC) and diluted appropriately to achieve ~10^8 CFU/ml.

Induction of diabetes and establishment of infection in wounds

A total of 48 Swiss albino mice (male and female, 12 weeks) were used for all experiments. Diabetes was induced by injecting multiple doses of Streptozotocin (STZ; Sigma-Aldrich Chemicals, USA) intraperitoneally according to the protocol, described in [23]. The blood glucose concentration was measured by a commercial glucometer (One-Touch Horizon, Johnson and Johnson) for 3 months to ensure sustained hyperglycemia. Mice with blood glucose level of >250 mg/dl were considered as diabetic. The diabetic mice at 4 weeks post STZ treatment and the corresponding gender, age-matched nondiabetic mice were used for wound creation. For this, in mice anesthetized by intraperitoneal injection of Ketamine (80 mg/kg) and Xylazine (10 mg/kg; Sigma-Aldrich Chemicals, USA) cocktail, the dorsal skin was shaved, treated with a depilatory cream, and then cleaned with povidone-iodine solution followed by 70 % alcohol wipe. Single wound (~1.5×1 cm) was created at the back of each mouse by excising the skin down to panniculus carnosus, using sterile surgical scissors and forceps [5, 6].

For the development of infection in wounds, ~10^7 CFU of exponential phase MRSA were applied topically onto each wound of diabetic mice and bacteria were allowed to grow for 48 h (day 2 post-wounding (p.w.). Signs of infection like purulent discharge, redness, and swelling were observed on day 2 p.w., suggesting development of infection in wounds.

Photodynamic therapy and other treatment of wounds

Cp6 was prepared in house following the procedure described in [14], and the drug was conjugated with cp6 by carbodiimide coupling method described in [5]. All the mice with wounds were divided into following groups: (1) uninfected, (2) uninfected, PDT given once on day 2 p.w., (3) infected untreated control, (4) infected, PDT given at 24-h intervals during days 1 to 3 p.w. (multiple PDT), (5) infected $AgNO_3$ and (6) infected AG. For carrying out PDT, 20 μl of 200 μM pl-cp6 was applied topically onto wounds. After 30 min of pl-cp6 application, wounds were exposed to red light (660±25 nm) using light source LC-122A (Citek, USA) at a power density of ~100 mW/cm^2, for 10 and 20 min, to achieve light fluence of ~60 and ~120 J/cm^2, respectively. For the infected PDT (multiple) group, light fluence of ~60 J/cm^2 was used.

AG was injected intraperitoneally at a dose of 100 mg/kg 1 day prior to wound creation and during days 1–3 p.w. [20]. In the $AgNO_3$ group, 10 μl of 0.5 % $AgNO_3$ [22] was applied onto wounds topically at 24-h intervals during days 1–3 p.w.

On day 3 p.w., animals (treated and untreated) were euthanized and wound tissues containing the scab, granulation tissue were harvested using scissors and forceps. The harvested wound tissues were either used for bacterial load analysis immediately or snap frozen in liquid nitrogen and stored at −80 °C for experiments requiring measurements on other biomarkers.

To determine bacterial load, wound tissues were homogenized (3500 rpm, 5 min) in phosphate-buffered saline (five times, *w*/*v*). The supernatant collected after centrifugation (10,000×*g*, 10 min) was plated on TSA agar plates. After incubation (24 h, 37 °C in dark), the number of colonies in each plate was counted. Bacterial load was determined by multiplying the number of colonies with dilution factor and volume of supernatant obtained during the tissue homogenization and was expressed as log CFU/wound [24].

Nitrite measurement in tissue lysate

For measurements on nitrite level, the tissues were first pulverized in liquid nitrogen with the help of a mortar/pestle. The tissue fragments were mixed (1:5, *w*/*v*) with 0.1 M chilled potassium phosphate buffer (pH 7.4), homogenized (3500 rpm, 5 min), and then sonicated at ~20 kHz, 10 s for four times, with gap of 10 s (Model CPX 130, Cole Parmer, USA). The supernatant collected after centrifugation (10, 000 rpm, 10 min) was used for measuring nitrite level using Griess reagent according to the protocol described in [25] with some modifications. Briefly, the tissue supernatant (50 μl) was mixed (1:1, *v*/*v*) with freshly prepared Griess reagent (0.1 % *N*-(1-naphthyl)ethylenediamine dihydrochloride, 1 % sulphanilamide, and 5 % phosphoric acid in a 1:1:1 ratio) and incubated for 30 min at 37 °C, in a 96-well microwell plate. Absorbance of the reaction product was measured at 545 nm using a microplate reader (Power Wave X340, Bio-Tek Instruments Inc, USA). The total protein content of the

wound lysate was estimated by bicinchoninic acid assay [26], using bovine serum albumin as standard. The NO levels of samples were determined by comparing with a calibration curve prepared using known concentration of sodium nitrite and NO level was expressed as micrograms of nitrite per milligram of protein.

VEGF-A measurement in tissue lysate

VEGF-A in the tissue lysate was measured using ELISA kit (Sigma-Aldrich, USA). Briefly, the powdered tissues were mixed with lysis buffer provided along with the ELISA kit and kept on ice for 30 min. The lysates were sonicated ("Nitrite measurement in tissue lysate") by keeping on ice and then centrifuged (5000 rpm, 10 min, 4 °C). The sample supernatant of each group was mixed (1:1, *v*/*v*) with a sample diluent buffer and incubated in the capture antibody-coated microwells provided with the kit, for 18 h at 4 °C. The assay was carried out according to the protocol described in the kit, and absorbance was recorded at 450 nm using a microplate reader. The tissue VEGF-A concentration was calculated from a standard curve prepared using the absorbance values of known concentrations of VEGF-A (10 pg–10 ng/ml), normalized with the protein content, and expressed as picograms per milligram of protein.

Estimation of stress signaling response markers in tissue lysate

The level of phospho-IKB-α, NF-kB p65, phospho-NF-kB p65, and phospho-p^{38} MAPK in the tissue lysate were estimated using multi-analyte ELISA kit (PATH SCAN ELISA Kit, Cell Signaling Technology, USA) following the protocol described by the manufacturer. The wound tissue lysate was prepared as described above ("Nitrite measurement in tissue lysate" and "VEGF-A measurement in tissue lysate"). The absorbance values of samples were normalized with protein content [26] and expressed as OD per milligram of tissue protein [5].

Determination of DNA content of wounds

The color reaction of deoxyribose with diphenylamine DNA content of the wound tissues were measured following the protocol described in ref. [25] with some modifications. Briefly, wound tissues were homogenized in 2 N HCl (1: 5, *w*/*v*), and the homogenate was incubated at 75 °C for 30 min in a water bath and then centrifuged (845 g, 20 min). The supernatant (0.5 ml) was mixed with 1 ml of diphenylamine reagent (1.5 g diphenylamine dissolved in 100 ml acetic acid and 1.5 ml sulfuric acid) and boiled in a water bath (95 °C) for 10 min. Absorbance of the colored product was measured at 600 nm in a spectrophotometer (Cintra 20, GBC Corp). The amount of DNA was determined by comparing calibration curve prepared using the absorbance of DPA and known concentrations (0.05–0.5 mg/ml) of calf thymus DNA (Bangalore Genei, India). The DNA concentration of the tissue lysates (mg/ml) obtained from the standard curve was normalized with the dry weight of tissue and expressed as milligrams of DNA per gram of tissue weight.

Wound closure

Mean wound closure time was determined as the time point (day) when the wound was devoid of any visible crust on the surface [5].

Statistical analysis

Data were analyzed and expressed as mean±standard deviation. Statistical comparison between means was carried out using one-way ANOVA. To quantify the correlation between the different parameters, the regression coefficient *R* from the linear regression analysis was used. $p<0.05$ were considered significant.

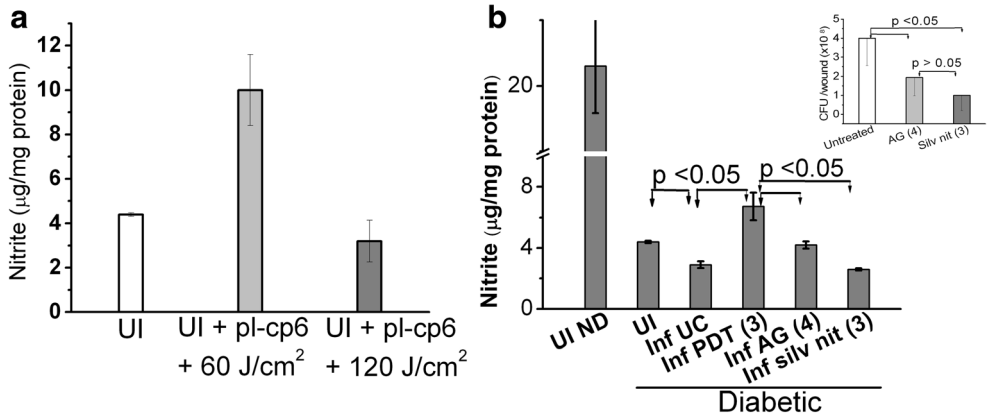

Fig. 1 **a** Effect of PDT fluence on NO level of wounds of diabetic mice on day 3 p.w. **b** Effect of topical APDT and other treatments on nitrite level of infected wounds of diabetic mice on day 3 p.w. Fig. 1b: inset; Bacterial load of wounds. Treatment frequencies for each group are denoted in parentheses, on *x*-axis. *UI* uninfected wounds, *Inf* infected wounds, *UC* untreated control, *ND* wound, nondiabetic mice. PDT (3) refers to multiple PDT fluence of ~60 J/cm^2

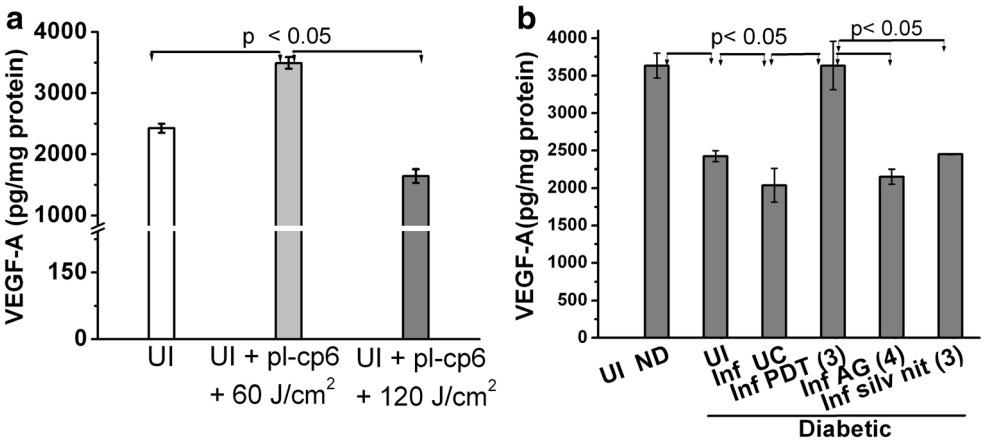

Fig. 2 **a** Effect of PDT fluence on VEGF-A level of wounds of diabetic mice on day 3 p.w. **b** Effect of topical APDT and other treatments on VEGF-A level of wounds of diabetic mice on day 3 p.w. Treatment frequencies for each group are denoted in parentheses, on *x*-axis. *UI* uninfected, *Inf* infected wounds, *UC* untreated control, *ND* wound, nondiabetic mice. PDT (3) refers to multiple PDT fluence of ~60 J/cm^2

Results

Effect of APDT on total nitrite content of wounds

In Fig. 1a, we show the results on NO level of uninfected wounds of diabetic mice exposed to single APDT at fluence ~60 and 120 J/cm^2. As shown in Fig. 1a, the level of NO in wounds treated with PDT at a light fluence of ~60 J/cm^2 increased significantly (by ~1.5 fold), whereas in wounds exposed to higher light fluence (~120 J/cm^2), their level decreased by ~1.5-fold. It should be noted that for the infected wounds, the multiple PDT protocol at lower light fluence (~60 J/cm^2) was used to maximize the bacterial inactivation and to reduce bacterial regrowth and damage to the inflammatory and other cells of the wound tissue. The results in Fig. 1b show the comparison of NO levels in wounds of the APDT, $AgNO_3$, and AG treatment groups. In MRSA-infected wounds, multiple APDT resulted in a significant increase in NO level. The level of NO in $AgNO_3$ treated wounds did not show significant change as compared with the wounds of untreated control group, although there was a significant reduction in bacteria (Fig. 1b, inset).

Effect of APDT on VEGF-A content of wounds

In Fig. 2a, we present the results on VEGF-A level in uninfected wounds of diabetic mice exposed to single APDT fluence of ~60 or 120 J/cm^2. As seen in the figure, the level of VEGF-A in response to PDT was similar to that of the changes observed for NO level. In infected wounds subjected to multiple PDT, the level of VEGF-A was observed to increase by ~1.75-fold as compared with the untreated controls. However, in wounds treated with $AgNO_3$ and AG (Fig. 2b), the VEGF-A level was significantly lower than for APDT. These results were also qualitatively similar to PDT response on NO level (Fig. 1).

Effect of PDT on NF-kB and p38 MAPK in wounds of diabetic mice

In Fig. 3, we show the results of our measurements on phospho-IKB-α, NF-kB p65, phospho-NF-kB p-65, and phospho-p38 MAPK levels in infected wounds of diabetic mice subjected to APDT, AG, and $AgNO_3$ treatment. While the infected wounds showed significantly higher levels of NF-kB p65, phospho-NF-kB p-65, and phospho-p38 MAPK, exposure of these wounds to PDT led to their downregulation. Further, levels of these markers in wounds of the three treatment groups followed the order APDT<AG<$AgNO_3$. In fact, it was observed that in the $AgNO_3$ group, the level of inflammatory markers were higher than the levels found in the untreated control group.

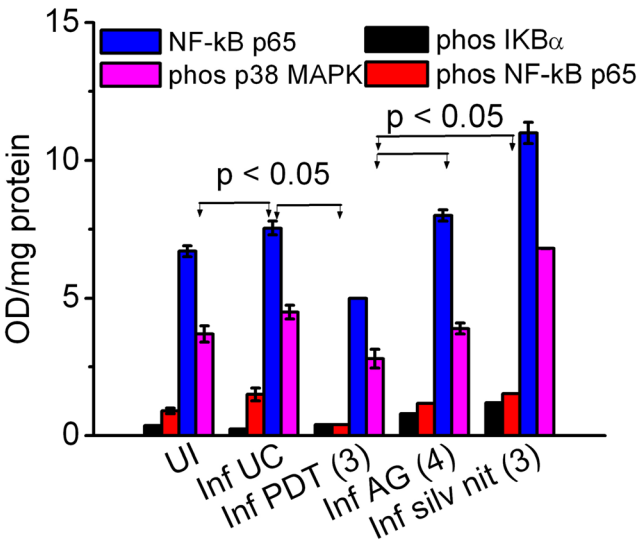

Fig. 3 Effect of APDT on biomarkers of stress signaling response of MRSA-infected wounds of diabetic mice on day 3 p.w. Treatment frequencies for each group are denoted in parentheses, on *x*-axis. *UI* uninfected wounds, *Inf* infected wounds, *UC* untreated control, *ND* wound, nondiabetic mice. PDT (3) refers to multiple PDT fluence of 60 J/cm^2

Table 1 Effect of PDT on DNA and protein contents of MRSA-infected wounds of diabetic mice on day 3 p.w.

	DNA content (mg/g wound tissue)	Protein content (mg/ml)
Uinfected	10–12	18–22
Untreated infected	15–20*	25–30*
Infected+PDT	24–28**	35–45*

Values present data of three experiments

*$p<0.05$, one-way ANOVA, compared with uninfected group; **$p<0.05$, compared with untreated group

Effect of APDT on DNA and protein content

The results in Table 1 show that in MRSA-infected wounds of diabetic mice subjected to multiple APDT, the DNA and protein contents increased significantly ($p<0.05$), compared with their untreated counterparts.

Correlation of wound NO, VEGF, and wound closure

Figure 4a shows a correlation between NO and VEGF-A levels in wound with wound closure. A good positive correlation ($R=0.8$) between wound tissue NO and VEGF-A level (Fig. 4a) was observed. Also, the wound closure time decreased with increase in NO level (Fig. 4b).

Discussion

It is known that impairment of wound healing in diabetes is caused by several systemic and local abnormalities. One important factor is reduced angiogenesis due to microangiopathy and vasculogenesis [10–12]. Since previous studies have demonstrated that ROS produced in response to hypoxia or ischemia, play important role in angiogenesis [27], it was of interest to investigate whether APDT-induced oxidative stress modulates angiogenesis in wounds of diabetic mice.

The results presented in this study (Figs. 1b and 2b) show that level of both the angiogenic markers (NO, VEGF-A) in the wounds of diabetic mice are significantly lowered compared with that of nondiabetic mice. This may be due to impairment of NO production and inducible nitric oxide synthase (iNOS) activity due to hyperglycemia-induced depletion of NADPH [28, 29]. The enhancement in angiogenic markers (NO, VEGF-A) observed in diabetic mice in response to PDT (Figs. 1a and 2a), could occur due to increase iNOS [28–30], release of protein-bound NO [31], and activation of hypoxia inducible factor VEGF signaling pathway [27]. However, these responses were reversed at the high APDT fluence, possibly due to the higher oxidative stress-induced damage to inflammatory cells [32]. Our results are consistent with previous studies wherein it has been shown that PDT-induced angiogenic response in tumors is light fluence dependent [13]. Increase in blood vessel formation has also been reported during PDT [33, 34].

It is known that *S. aureus* infection can delay angiogenesis [35] by inducing prolonged presence of neutrophils [36, 37], apoptosis in macrophages [38], downregulated VEGF signaling [39], and reduced VEGF stability in the wound environment [35]. Therefore, the observations of APDT-induced increase in VEGF-A and NO levels in infected wounds could be due to inactivation of *S. aureus* toxins such as the alpha toxins and other proteases which would result in higher macrophage recruitment to the wound site. This increased NO, produced by macrophages, in a feedback loop would lead to more VEGF-A as well as contribute to macrophage accumulation at the wound site. It is also important to note that in addition to increase in proangiogenic response, APDT also led to increase in DNA and protein contents (Table 1) of the infected wounds subjected to PDT, compared with their untreated controls. It is pertinent to note that this increase cannot be accounted for by the increased

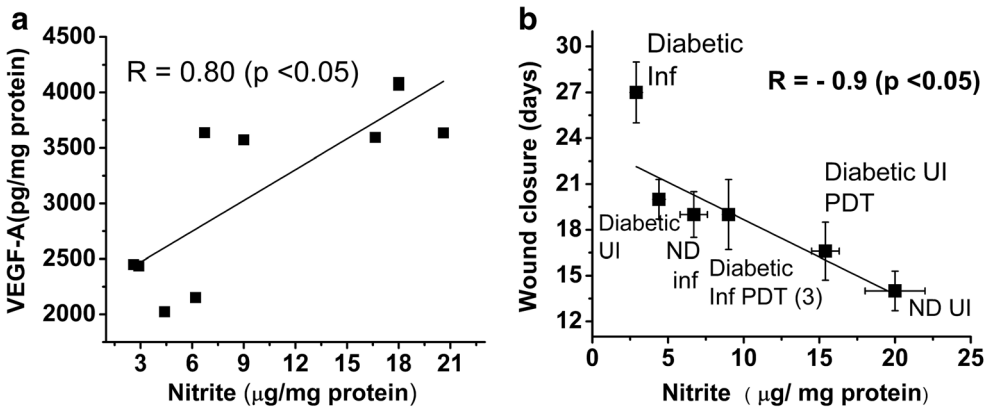

Fig. 4 **a** Correlation of wound NO versus VEGF-A in diabetic mice ($n=9$). **b** Effect of APDT-induced increased nitrite level on wound closure of MRSA-infected wounds of nondiabetic and diabetic mice. *UI* uninfected wounds, *Inf* infected wounds, *UC* untreated control, *ND* wound, nondiabetic mice. PDT (3) refers to multiple PDT fluence of 60 J/cm^2

bacteria content. The protein content of a single bacterium is only 50–300 fg [40] and even bacterial load as high as 10^9 CFU/wound would contribute only ~0.3 mg increase in the total protein content of the wound. This is insignificant considering the magnitude of increase (~4–5 mg) in protein content observed for the infected wounds. Further, compared with untreated infected wounds, DNA and protein contents in the infected wounds subjected to PDT are significantly higher (Table 1), in spite of the ~1.5 log decrease in bacterial load (Fig. 1b, inset). Therefore, the increased DNA/protein contents of the wounds suggest increase in host cell proliferation. This is consistent with the faster closure of wounds in photodynamically treated group (Fig. 4b).

Further, the results show down regulation of NF-kB p65, phos-NF-kB p65 by PDT which is expected to be due to the destruction of bacteria and the moderate enhancement in NO [18]. NF-kB and p38 MAP kinase (MAPK) participate in signaling cascade controlling the cellular response to proinflammatory stress during hyperglycemia, bacteria infection, and overexpression of these proteins can lead to inhibition of wound closure [15] by various ways such as prolonged inflammation [10, 11, 15] by extending neutrophil half life [41], inhibition of angiogenesis [42, 43], upregulation of matrix metalloproteases (MMPs) [16], and bacterial invasion [41]. Therefore, downregulation of NF-kB and p38 MAPK levels of wounds, on day 3 p.w. can lead to beneficial response such as reduction in neutrophil number [41], increased angiogenesis [42, 43], inhibition of bacteria growth [41], and improved wound closure [15].

Our study also shows that among the three treatment groups, a reduction in inflammatory response is observed only in the APDT group; though both AG, $AgNO_3$ treatments led to significant decrease in bacterial load. In fact, $AgNO_3$ led to enhancement of inflammatory markers. This is in agreement with induction of acute inflammation by $AgNO_3$ reported previously [44] and also because $AgNO_3$ does not have any effect on bacterial toxins. Although AG is expected to reduce inflammation and promote wound healing by inhibiting AGE in diabetic wounds [20, 21], it does not have any bactericidal effect like APDT.

Conclusion

Results presented in this study suggest that APDT enhances angiogenic response in the bacteria-infected wounds. Further, the results presented suggest that antibacterial effect of PDT-induced abrogation of hyperinflammatory response and enhancement of cell proliferation results in faster wound closure.

Acknowledgment The authors acknowledge help of Shri Anupam Chowdhury in establishment of wound infection and biochemical measurements.

Conflict of interest The authors declare that they have no conflict of interest.

Ethics statement All the experimental procedures involving animals were approved by the Institutional Animal Ethics Committee, in accordance with the guidelines of the Committee for Purpose of Care and Supervision of Experimental Animals (CPCSEA), Department of Environment and Forests, Government of India. The animals were housed individually in cages with free access to food and water and maintained on a 12-h light/dark cycle at 22 °C (±2 °C). All the animal manipulations involving wounds were carried out in anesthetized conditions, and animals were kept on warm cotton pads for recovery from anesthesia. Animals were euthanized by cervical dislocation. All research animals were treated humanely, and all efforts were made to minimize the animal suffering and the number of animals killed.

References

1. Maisch T (2009) A new strategy to destroy antibiotic resistant microorganisms: antimicrobial photodynamic treatment. Mini Rev Med Chem 9:974–983
2. Hashimoto MC, Prates RA, Kato IT, SC N´ n˜ e, Courrol LC, Ribeiro MS (2012) Antimicrobial photodynamic therapy on drug resistant *Pseudomonas aeruginosa* induced infection. An in vivo study. Photochem Photobiol 88:590–595
3. Vecchio D, Dai T, Huang L, Fantetti L, Roncucci G, Hamblin MR (2013) Antimicrobial photodynamic therapy with RLP068 kills methicilin resistant *Staphylococcus aureus* and improves wound healing in a mouse model of infected skin abrasion. J Biophotonics 6:733–742
4. Sharma M, Bansal H, Gupta PK (2005) Virulence of *Pseudomonas aeruginosa* cells surviving photodynamic treatment with toluidine blue. Curr Microbiol 50:277–280
5. Sahu K, Sharma M, Bansal H, Dube A, Gupta PK (2013) Topical photodynamic treatment with poly-L-lysine-chlorin p6 conjugate improves wound healing by reducing hyperinflammatory response in *Pseudomonas aeruginosa* infected wounds of mice. Lasers Med Sci 28:465–471
6. Sahu K, Sharma M, Sharma P, Verma Y, Rao KD, Bansal H, Dube A, Gupta PK (2014) Effect of poly-L-lysine-chlorin p6-mediated antimicrobial photodynamic treatment on collagen restoration in bacteria-infected wounds. Photomed Laser Surg 32:23–29
7. Morley S, Griffiths J, Philips G, Moseley H, O'Grady C, Mellish K, Lankester CL et al (2013) Phase IIa randomized, placebo-controlled study of antimicrobial photodynamic therapy in bacterially colonized, chronic leg ulcers and diabetic foot ulcers: a new approach to antimicrobial therapy. Br J Dermatol 168:617–624
8. Tardivo JP, Adami F, Correa JA, Pinhal MA, Baptista MS (2014) A clinical trial testing the efficacy of PDT in preventing amputation in diabetic patients. Photodiagnosis Photodyn Ther 11:342–350
9. Mannucci E, Genovese S, Monami M, Navalesi G, Dotta F, Anichini R et al (2014) Photodynamic topical antimicrobial therapy for infected foot ulcers in patients with diabetes: a randomized, double-blind, placebo-controlled study—the D.A.N.T.E (Diabetic ulcer Antimicrobial New Topical treatment Evaluation) study. Acta Diabetol 51:435–440
10. Brownlee M (2001) Biochemistry and molecular cell biology of diabetic complications. Nature 414:813–820

11. Brem H, Tomic-Canic M (2007) Cellular and molecular basis of wound healing in diabetes. J Clin Invest 117:1219–1222
12. Costa PZ, Soares R (2013) Neovascularization in diabetes and its complications. Unraveling the angiogenic paradox. Life Sci 92: 1037–1045
13. Zhang X, Jiang F, Kalkanis SN, Zhang Z, Hong X, Yang H, Chopp M (2007) Post-acute response of 9L gliosarcoma to Photofrin-mediated PDT in athymic nude mice. Lasers Med Sci 22:253–259
14. Hoober JK, Sery TW, Yamamoto N (1988) Photodynamic sensitizers from chlorophyll: purpurin-18 and chlorin p6. Photochem Photobiol 48:579–582
15. Medicherla S, Wadsworth S, Cullen B, Silcock D, Ma JY, Mangadu R, Kerr I et al (2009) p38 MAPK inhibition reduces diabetes-induced impairment of wound healing. Diabetes Metab Syndr Obes 2:91–100
16. Zhu P, Ren M, Yang C, Hu YX, Ran JM, Yan L (2012) Involvement of RAGE, MAPK and NF-κB pathways in AGEs-induced MMP-9 activation in HaCaT keratinocytes. Exp Dermatol 21:123–129
17. Bien J, Sokolova O, Bozko P (2011) Characterization of virulence factors of *Staphylococcus aureus*: novel function of known virulence factors that are implicated in activation of airway epithelial proinflammatory response. J Pathog 2011:601905
18. Son Y, Cheong YK, Kim NH, Chung HT, Kang DG, Pae HO (2011) Mitogen-activated protein kinases and reactive oxygen species: how can ROS activate MAPK pathways? J Signal Transduct 2011:792639
19. Kelleher ZT, Matsumoto A, Stamler JS, Marshall HE (2007) NOS2 regulation of NF-kappaB by S-nitrosylation of p65. J Biol Chem 282:30667–306772
20. Ozturk A, Fırat C, Parlakpınar H, Bay-Karabulut A, Kirimlioglu H, Gurlek A (2012) Beneficial effects of aminoguanidine on skin flap survival in diabetic rats. Exp Diabetes Res 2012:721256
21. Tian M, Qing C, Niu Y, Dong J, Cao X, Song F, Ji X, Lu S (2013) Effect of aminoguanidine intervention on neutrophils in diabetes inflammatory cells wound healing. Exp Clin Endocrinol Diabetes 121:635–642
22. Atiyeh BB, Costagliola M, Hayek SN, Dibo SA (2007) Effect of silver on burn wound infection control and healing: review of the literature. Burns 33:139–148
23. Arora S, Ojha SK, Vohora D (2009) Characterisation of streptozotocin induced diabetes mellitus in Swiss albino mice. Global J Pharmacol 3:81–84
24. Zhao G, Usui ML, Underwood RA, Singh PK, James GA, Stewart PS et al (2012) Time course study of delayed wound healing in a biofilm-challenged diabetic mouse model. Wound Repair Regen 20:342–352
25. Jagetia GC, Rajanikant GK, Mallikarjun Rao KV (2007) Ascorbic acid increases healing of excision wounds of mice whole body exposed to different doses of gamma-radiation. Burns 33:484–494
26. Smith PK, Krohn RI, Hermanson GT, Mallia AK, Gartner FH, Provenzano MD et al (1985) Measurement of protein using bicinchoninic acid. Anal Biochem 150:76–85
27. Kim YW, Byzova TV (2014) Oxidative stress in angiogenesis and vascular disease. Blood 123:625–631
28. Luo JD, Chen AF (2005) Nitric oxide: a newly discovered function on wound healing. Acta Pharmacol Sin 26:259–64
29. Witte MB, Barbul A (2002) Role of nitric oxide in wound repair. Am J Surg 183:406–412
30. Song S, Zhou F, Chen WR, Xing D (2013) PDT-induced HSP70 externalization up-regulates NO production via TLR2 signal pathway in macrophages. FEBS Lett 587:128–135
31. Herold S, Boccini F (2006) NO* release from MbFe(II)NO and HbFe(II)NO after oxidation by peroxynitrite. Inorg Chem 45: 6933–6943
32. Tanaka M, Mroz P, Dai T, Huang L, Morimoto Y, Kinoshita M et al (2012) Photodynamic therapy can induce a protective innate immune response against murine bacterial arthritis via neutrophil accumulation. PLoS One 7, e39823
33. Jiang F, Zhang ZG, Katakowski M, Robin AM, Faber M, Zhang F, Chopp M (2004) Angiogenesis induced by photodynamic therapy in normal rat brains. Photochem Photobiol 79:494–498
34. Zhang X, Jiang F, Zhang ZG, Kalkanis SN, Hong X, Decarvalho AC, Chen J, Yang H, Robin AM, Chopp M (2005) Low-dose photodynamic therapy increases endothelial cell proliferation and VEGF expression in nude mice brain. Lasers Med Sci 20:74–79
35. Simonetti O, Cirioni O, Goteri G et al (2008) Temporin A is effective in MRSA-infected wounds through bactericidal activity and acceleration of wound repair in a murine model. Peptides 29:520–528
36. Frank H, Park S, Rich J, Lee JC (2011) Reduced neutrophil apoptosis in diabetic mice during staphylococcal infection leads to prolonged TNFα production and reduced neutrophil clearance. PLoS One 6, e23633
37. Shibata T, Nagata K, Kobayashi Y (2010) The mechanism underlying the appearance of late apoptotic neutrophils and subsequent TNF-α production at a late stage during *Staphylococcus aureus* bioparticle-induced peritoneal inflammation in inducible NO synthase deficient mice. Biochim Biophys Acta 1802:1105–1111
38. Im SS, Osborne TF (2012) Protection from bacterial toxin induced apoptosis in macrophages requires the lipogenic transcription factor sterol regulatory element binding protein 1a. Mol Cell Biol 32: 2196–2202
39. Power C, Wang JH, Sookai S, Street JT, Redmond HP (2001) Bacterial wall products induce down-regulation of vascular endothelial growth factor receptors on endothelial cells via a CD14-dependent mechanism: implications for surgical wound healing. J Surg Res 101:138–145
40. Zubkov MV, Fuchs BM, Eilers H, Burkill PH, Amann R (1999) Determination of total protein content of bacterial cells by SYPRO staining and flow cytometry. Appl Environ Microbiol 65:3251–3257
41. Ipaktchi K, Mattar A, Niederbichler AD, Hoesel LM, Vollmannshauser S, Hemmila MR et al (2007) Topical p38 MAPK inhibition reduces bacterial growth in an in vivo burn wound model. Surgery 142:86–89
42. Ho FM, Lin WW, Chen BC, Chao CM, Yang CR, Lin LY et al (2006) High glucose induced apoptosis in human vascular endothelial cells is mediated through NF-kappaB and c-Jun NH2-terminal kinase pathway and prevented by PI3K/Akt/eNOS pathway. Cell Signal 18:391–399
43. Tabruyn SP, Griffioen AW (2008) NF-kappa B: a new player in angiostatic therapy. Angiogenesis 11:101–106
44. Marchi E, Vargas FS, Acencio MM, Antonangelo L, Teixeira LR, Light RW (2009) Low doses of silver nitrate induce pleurodesis with a limited systemic response. Respirology 14:885–889